LA-UR-82-1715

Conf-830103--13

Los Alamos National Laboratory is operated by the University of California for the United States Department of Energy under contract W-7405-ENG-36.

LA-UR--82-1715

DE82 018453

TITLE: FUEL PENETRATION OF INTERSUBASSEMBLY GAPS IN LMFBRS

AUTHOR(S): G. DeVault

SUBMITTED TO: Second International Topical Meeting on Nuclear Reactor Thermalhydraulics, January 11-14, 1983
Santa Barbara, California

MASTER

eb

Los Alamos Los Alamos National Laboratory
Los Alamos, New Mexico 87545

FORM NO 836 R4
ST NO 2629 5/81

FUEL PENETRATION OF INTERSUBASSEMBLY GAPS IN LMFBRS*

(A Calculational Method with the SIMMER-II Code)

by

G. P. DeVault**

ABSTRACT

Early fuel removal from the active core of a liquid-metal-cooled fast breeder reactor (LMFBR) undergoing a core-disruptive accident may reduce the potential for large energetics resulting from recriticalities. A possible avenue for early fuel removal in heterogeneous core LMFBRs is the failure of duct walls in disrupted driver subassemblies followed by fuel penetration into the gaps between blanket subassemblies. The SIMMER-II code was modiofied to simulate flow between subassembly gaps. Calculations with the modified SIMMER-II code indicate the capabilities of the method and the potential for fuel mass reduction in the active core.

---

*Work performed under the auspices of the US Department of Energy.
**Energy Division, Los Alamos National Laboratory, Los Alamos, NM 87545

I. INTRODUCTION AND SUMMARY

Possible avenues for fuel removal from the active core driver regions are important in considerations of hypothetical core-disruptive accidents (HCDA) in liquid-metal-cooled fast breeder reactors (LMFBR). Earlier SIMMER-II[1] calculations of the meltdown phase of such accidents in heterogeneous cores[2], such as the bull's-eye core of the Conceptual Design Study (CDS) reactor[3], have shown that a propensity for fuel slumping produces an active system response characterized by a series of prompt- or near prompt-critical power bursts. The number and severity of recriticalities are related directly to the availability of mobile fuel in the active core. Early fuel losses can eliminate or moderate recriticalities. Fuel losses from the core region to the axial blankets through normal coolant flow passages may occur because of high pressures during and after power bursts. However, prior cladding blockages and fuel freezing and plugging in those axial blanket passages may limit the effectiveness of that fuel removal path.

Another possibility for fuel removal is progressive failure of driver subassembly duct walls by a combination of pressure and heat flow from the hot fuel. To analyze the subsequent fuel penetration into gaps between blanket subassemblies, the SIMMER-II code has been modified. The modifications were an attempt to model as closely as possible the proper heat-flow and heat-capacity characteristics of the blanket subassembly duct walls and the sodium flow paths between adjacent subassembly duct walls.

To evaluate this model a preliminary calculation was made for a whole-core simulation of the CDS reactor. In this simulation the reactor had an outer annular driver region that had been disrupted previously and that contained a slumped pool of molten fuel and steel at 3100 K. The region

inside the annular core region was modeled as a nonparticipating region for convenience; below the pool was an intersubassembly gap region (that can be considered as a two-dimensional porous region with the gap channel being the porosity) and radially surrounding these regions was another assumed gap region--the radial blanket. A sodium leak path for the sodium initially in the gaps was provided at the top of the radial blanket to simulate the resistance represented by the subassembly load pads. Melt-through failure of subassembly duct walls separating the core pool from the radial blanket gap region initiated the flow of pool material into the radial gaps. Before this some flow into the lower gap region occurred. As pool material (consisting of 25% fuel particles, 25% liquid steel, and 50% liquid fuel at the time of wall failure) began moving into the radial blanket gaps, the liquid fuel partially froze on the structure but mostly it froze into particles. The particles were able to penetrate far into the gap region. In particular, by 3 s after wall failure, the total fuel mass in the slumped core had decreased 33%. This was sufficient to decrease significantly the probability of further recriticality. This potential for fuel removal is dependent on the various heat-transfer processes that are acting simultaneously. These processes affect the amounts and timing of fuel particle and fuel crust formation, sodium interaction and vaporization, and the availability of flow passages.

In summary, a tool is available for analyzing possible fuel removal from the active core region of an LMFBR by intersubassembly gap penetration within a whole-core analysis context. These escape paths for fuel from the core show sufficient promise to merit a more detailed and accurate analysis of their influence on the whole-core meltdown problem.

II. MODIFICATIONS TO SIMMER-II FOR TREATING INTERCONNECTED GAP FLOW

Typically SIMMER-II models an LMFBR reactor core in cylindrical coordinat with azimuthal symmetry. Usually a radial mesh cell will characterize several hexagonal subassemblies with a flow area representi the normal coolant flow areas through the pin bundles. However, we wished to consider, in the axial blanket portions of the driver subassemblies and in the blanket subassemblies, the flow paths represented by the interconnected gaps between the subassemblies in those regions. Because SIMMER-II can track only one flow path within a mesh cell, flow within these subassemblies (the pin bundles of the subassemblies) could not be treated simultaneously with the flow in the gaps.

The sodium ordinarily within these subassemblies will thermally couple the blanket pins and subassembly duct walls as well as convectively remove heat from the walls. Thus the pin bundle fluid dynamics was sacrificed on the basis that it is of importance only after the duct wall fails (gaps and pin bundles become connected) and as a boundary condition for the duct walls exposed to the gap fluid. To simulate this means of heat transfer and the effectively larger local heat capacity that results, that is, to keep the blanket subassembly duct walls from incurring unrealistically large temperature increases and subsequent premature failure, the walls in the porous regions were given an appropriate additional thickness. But because flow into the gaps of radial blanket was assumed to be initiated by partial melting at the duct walls at the interface, the SIMMER-II wall-failure model had to be modified to prevent unrealistic delayed failure.

III. ASSESSMENT OF GAP FUEL REMOVAL POTENTIAL

A. Geometric Arrangement and SIMMER-II Mesh

The SIMMER-II cylindrical mesh chosen for these calculations was adapted from the CDS heterogeneous core (Fig. 1). The total calculational system is shown in Fig. 2. In Fig. 2 the condenser, voided core, and initially slumped core represent the active core of the third driver ring of subassemblies. Interior to this region is a nonparticipating filler region. The radial blanket and shield region, labeled as porous, is a region where molten core material is allowed to flow in the intersubassembly gaps when the driver subassembly duct walls have failed. There are also porous lower subassemblies that provide for intersubassembly gap flow. In addition there are top and bottom leak paths that, according to their specified hydraulic diameters, provide means of escape for flowing materials.

B. Initial and Boundary Conditions

A whole-core calculation of an HCDA was performed recently for the heterogeneous CDS reactor[2]. For our initial conditions (t = 0 s) in this study we used coolant, cladding, fuel pellet, and subassembly duct wall axial temperature profiles produced in the previous CDS calculation at a time when driver ring 3 had been severely disrupted. Its fuel was in a slumped state but the subassembly duct walls of the low-power subassemblies at the radial blanket interface had not failed. Constant pressures of 0.1 and 0.122 MPa were applied at the top and bottom boundaries, respectively.

Figure 3 illustrates the spatial distributions of the initial states of the (a) subassembly duct wall macroscopic density and (b) its temperature, (c) the liquid fuel macroscopic density, and (d) the liquid sodium macroscopic density.

C. Results

In Section III.A and III.B a base case calculation is considered for which there was only an upper leak path. Deviations from the base case in which an additional leak path was provided and in which the liquid-liquid heat transfer was reduced are discussed in Section III.C.

1. Time Interval Before Wall Failure. Subassembly duct walls between the core and the radial blanket began to fail at t = 1.114 s by melting. However, before this time some liquid fuel and steel in the slumped core began to flow down into the porous regions below the core where it interacted with the sodium initially in the gaps. This fuel-steel-coolant interaction generated local pressures (Fig. 4) sufficient to cause the slumped core material to begin sloshing into the voided core and condenser regions (Fig. 5). In addition, considerable liquid sodium in the porous lower subassemblies vaporized (Figs. 6 and 7). Fuel particles were formed in the condenser region because the sloshing fuel reaching this colder region melted the cladding on the pin stubs thereby permitting the breakup of unclad, unsupported fuel pellets in this region. Also liquid fuel froze as crusts on subassembly duct walls in the outer voided core and in the porous lower assemblies (Fig. 8).

2. Time Interval After Wall Failure. Shortly after the subassembly duct walls began to fail, high pressure (Fig. 9a) was produced by fuel-coolant interaction near the wall failure site (Fig. 9b). This localized high pressure produced outward radial flow of liquid field material into the radial blanket porous gaps (Fig. 9d), displacing liquid sodium (Fig. 9c).

The pressure distribution gradually flattened with time (Fig. 10). Simultaneously liquid fuel in the driver both slumped back to the bottom of

the core and decreased in absolute amount with time (Fig. 11) as it was discharged from the core and was converted to fuel particulate by the cold entrained steel from the melting walls. After the wall failure, liquid fuel moved out into the porous radial blanket; some froze on the blanket subassembly duct walls near the failed wall opening (Fig. 12). Although some of the liquid sodium (Fig. 13) vaporized (Fig. 14), its decrease (60%) was mostly due to flow out the upper leak path.

Figures 15-17 give the time histories of several variables for various regions in the calculational mesh. The outer core driver subassembly duct wall began to fail at 1.1 s and was completely melted through by 2.1 s (Fig. 15a). When these walls failed, that liquid fuel that had frozen on the walls as a crust broke up into particles and became a part of the liquid field (Fig. 15b). The average pressure over this failed region reached a maximum of 3.6 MPa because of the interaction of the molten fuel and steel with the sodium coolant in the porous gap region (Fig. 15c). The fuel mass inventory in the disrupted core decreased by one third as it flowed into the porous regions (Fig. 15d). The liquid fuel mass in the gaps was continually cooled; about two-thirds formed particles in the flow stream and one-third froze on subassembly walls in the porous gaps as crusts (Figs. 16a-c). The total fuel mass inventory for the complete system decreased by 6% (Fig. 16d)--indicating that very little flowed out the upper leak path although 60% of the liquid sodium in the gaps was ejected during this time.

Steel also flowed into the porous gap region where a small amount froze onto subassembly duct walls but most formed additional particles (Figs. 17a-b). Because of the freezing and plugging in the gaps the effective hydraulic diameters in the porous regions decreased with time (Figs. 17c-d).

However, this decrease was small and amounted to only 14% in the porous radial blanket.

3. Effects of Leak Paths and Liquid Heat-Transfer Coefficients. Some additional complete cases were calculated to investigate the following: (a) the effect on the driver fuel removal produced by an additional leak path; (b) the effect of reducing the liquid-liquid heat transfer on the possible over-prediction of the fuel-coolant interaction.

A leak path was added at the bottom outer radial mesh cell by giving that cell the properties of the porous regions. A SIMMER-II calculation through 4 s of problem time showed that, as compared to the base case, this additional leak path gave a 50% loss of fuel from the driver region; over twice as much fuel flowed out of the system; half as many fuel particles remained in the porous regions; and 50% more refrozen fuel remained in the porous regions. Also only half as much liquid sodium remained in the system as did in the base case. This indicates that the ease of sodium ejection may be significant to this fuel removal process.

In another calculation, the liquid-liquid heat-transfer coefficients were reduced by a factor of one hundred. In this case the SIMMER-II calculation showed that although almost as much fuel was removed from the driver core as in the base case, considerably less was removed from the system.

A calculation was also made that incorporated both the above changes. Rather surprisingly this calculation indicated that 58% of the fuel was removed from the driver core and 22% of the fuel left the system. The results of these three cases, relative to the base case, are given in Table I.

IV. CONCLUSIONS

An improvement to SIMMER-II has been developed for analyzing fuel removal from LMFBR active core regions by intersubassembly gap penetration. Preliminary calculations generated initial coolant interaction with molten fuel and steel after subassembly duct wall failure creating pressures of the order of tens of atmospheres. This was followed by driver core fuel and some steel being driven into the porous gap regions. The mixture of fuel particulate and liquid steel flowed deep into the porous regions. Some of the particles flowed out through leak paths but most remained in the gap regions. Because the fuel throughout the porous regions was in a particulate form and the liquid steel was generally above its freezing temperature, extensive plugging did not occur. The results gave a strong indication that fuel escape from a severely disrupted core via intersubassembly radial blanket gaps may indeed be an important means of limiting further recriticalities.

Future considerations of this method are planned to include whole core analyses of heterogeneous LMFBRs such as the Clinch River Breeder Reactor.

REFERENCES

1. Smith, L. L., "SIMMER-II: A Computer Program for LMFBR Disrupted Core Analysis," Los Alamos Scientific Laboratory report NUREG/CR-0453, LA-7515-M, Oct. 1978.

2. Luck, L. B., et al., "A Transition-Phase Calculation of a Large, Heterogeneous Core LMFBR," Trans. Am. Nuc. Soc., San Francisco, Nov. 29-Dec. 4, 1981.

3. Mills, J. C., "Transmittal of AI Heterogeneous Core Design Information," Atomics International letter to L. L. Smith, May 18, 1979.

TABLE I

COMPARISON OF CALCULATED RESULTS FOR MODIFIED ASSUMPTIONS RELATIVE TO BASE CASE

	Base Case	(a) Additional Leak Path	(b) Liquid-Liquid Heat Transfer Reduced by 10^{-2}	(a) and (b) Combined
Fuel Removed from Core	1.	1.48	1.34	1.70
Fuel Removed from System	1.	2.67	0.56	3.89
Refrozen Fuel in Gaps	1.	1.55	1.77	2.74
Fuel Particles in Gaps	1.	0.51	1.06	0.49
Steel Particles in Gaps	1.	0.45	0.06	0.01

List of Figures

Fig. 12. Fuel crust macroscopic density (kg/m^3) at selected times.

Fig. 13. Liquid sodium macroscopic density (kg/m^3) at selected times.

Fig. 14. Sodium vapor macroscopic density (kg/m^3) at selected times.

Fig. 15. Time histories of selected variables.

Fig. 16. Time histories of selected variables.

Fig. 17. Time histories of selected variables.

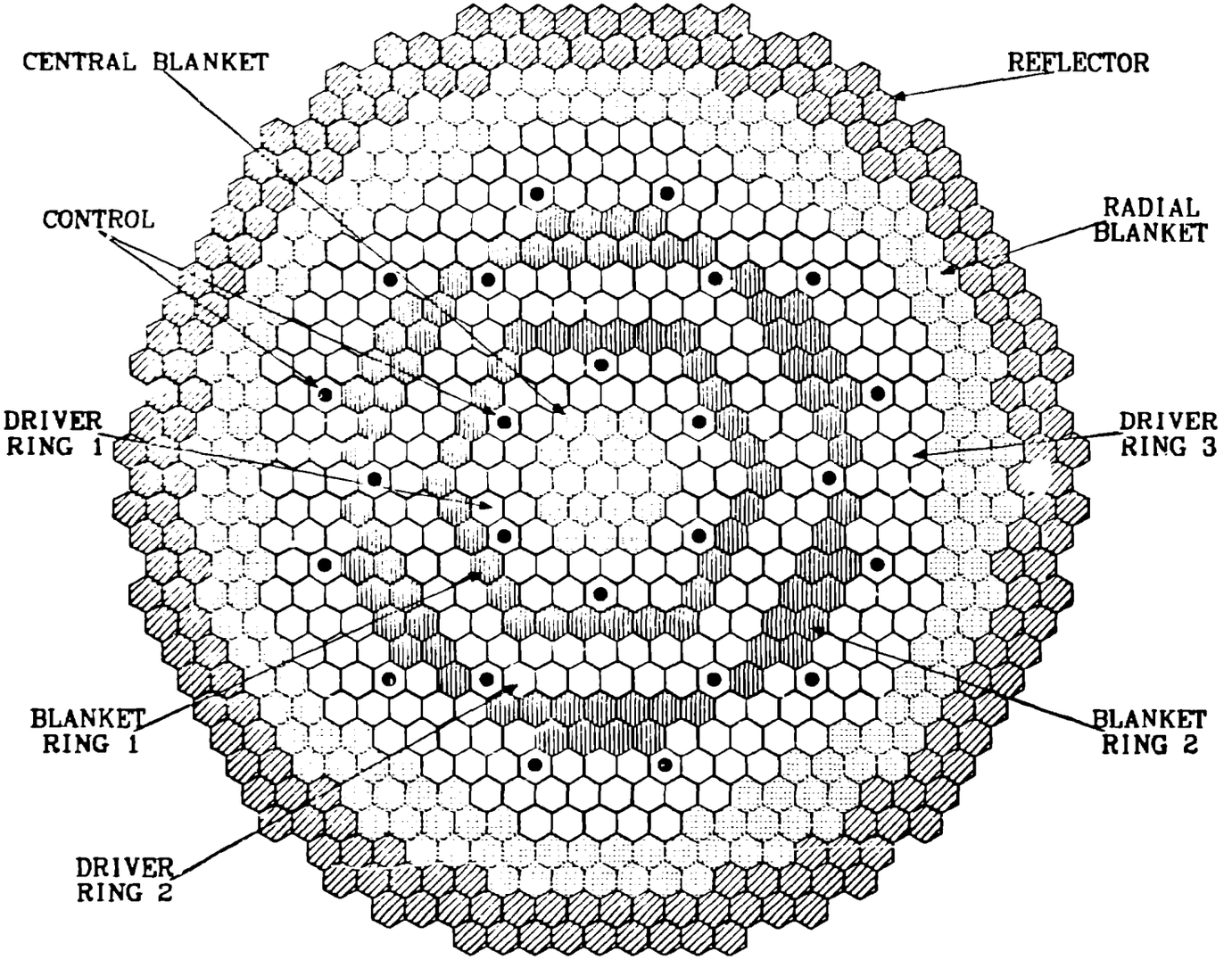
CENTRAL BLANKET
REFLECTOR
CONTROL
RADIAL BLANKET
DRIVER RING 1
DRIVER RING 3
BLANKET RING 1
BLANKET RING 2
DRIVER RING 2

Fig. 1.

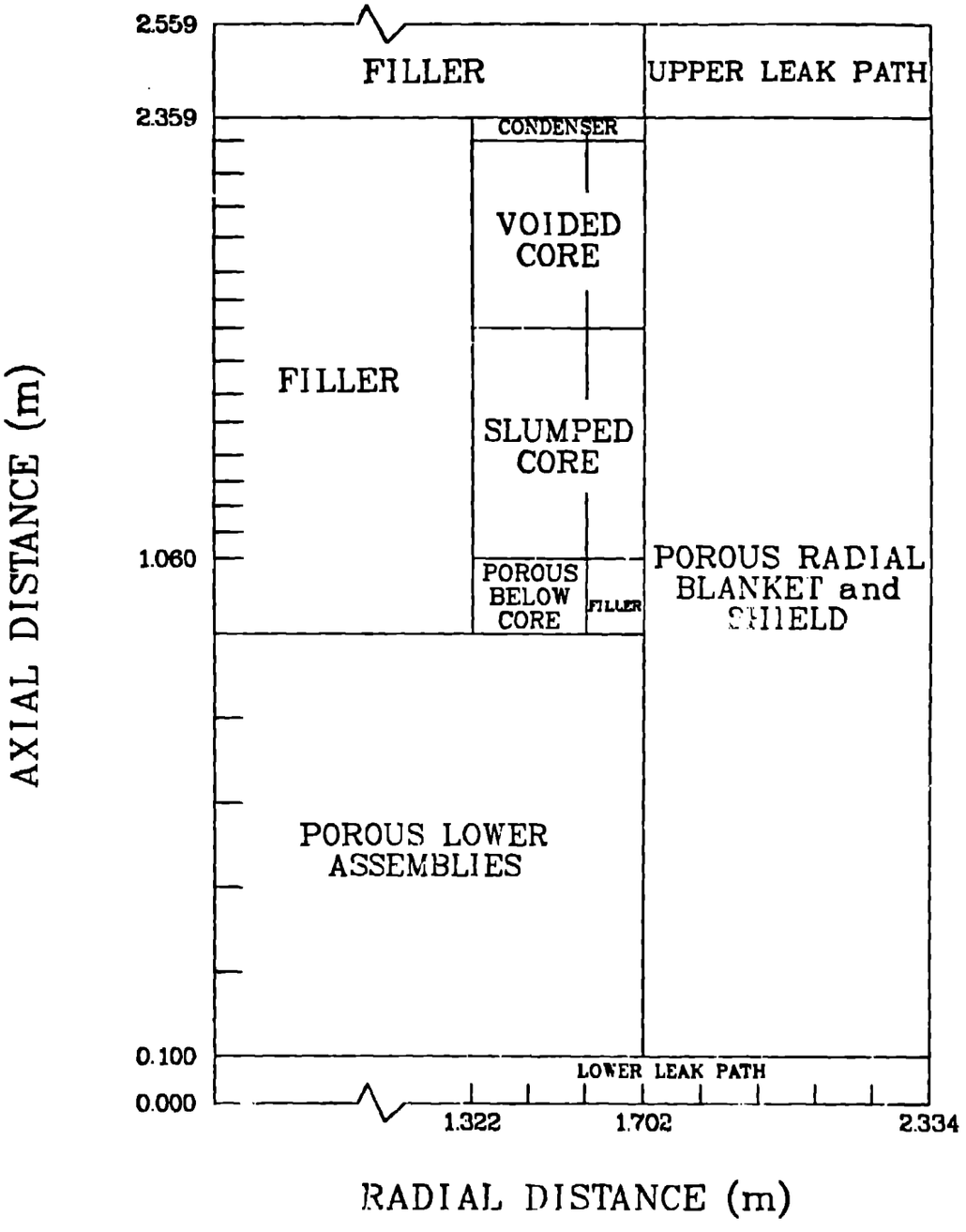
2.559
2.359
1.060
0.100
0.000
FILLER
UPPER LEAK PATH
CONDENSER
VOIDED CORE
FILLER
SLUMPED CORE
POROUS BELOW CORE
FILLER
POROUS RADIAL BLANKET and SHIELD
POROUS LOWER ASSEMBLIES
LOWER LEAK PATH
1.322
1.702
2.334
AXIAL DISTANCE (m)
RADIAL DISTANCE (m)

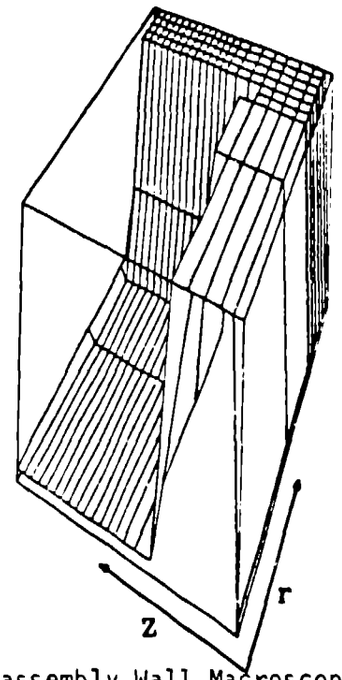

(a) Subassembly Wall Macroscopic Density (kg/m^3)
(Min = 0., Max = 7792.)

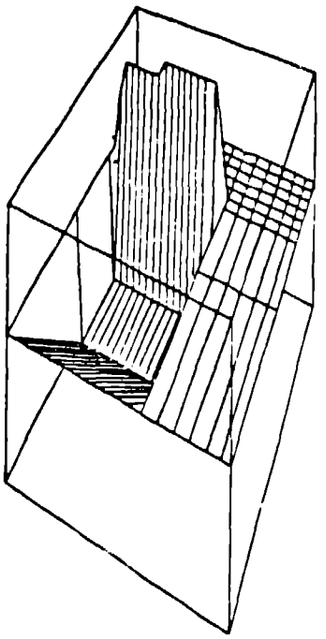

(b) Subassembly Wall Temperature (k)
(Min = 0., Max = 1500.)

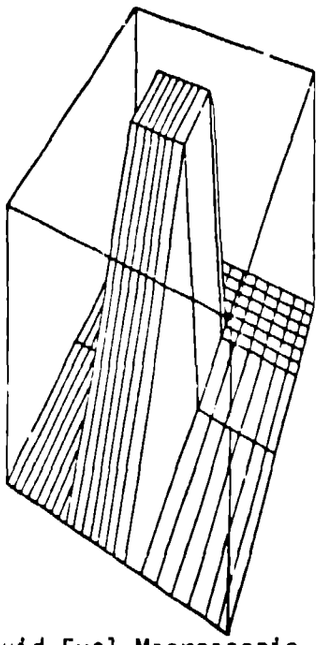

(c) Liquid Fuel Macroscopic Density (kg/m^3)
(Min = 0., Max = 5976.)

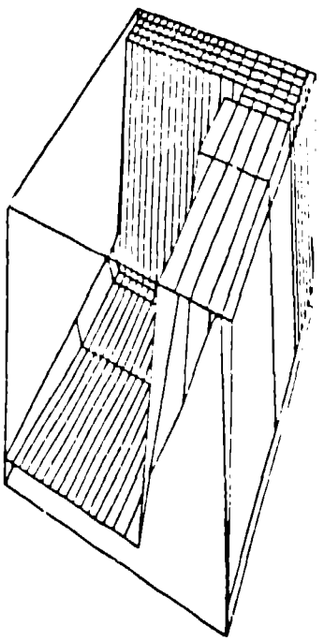

(d) Liquid Sodium Macroscopic Density (kg/m^3)
(Min = 0., Max = 70.2)

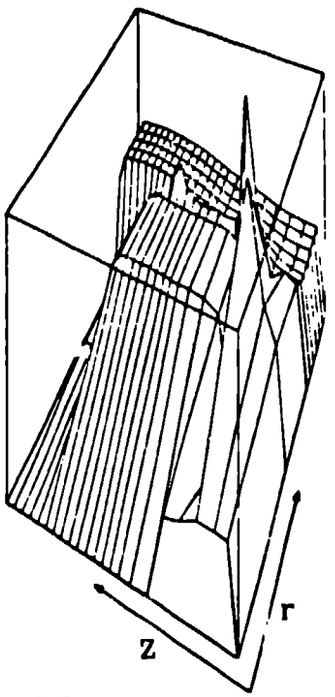

t = 0.1 s
(Min = 0.100, Max = 0.544)

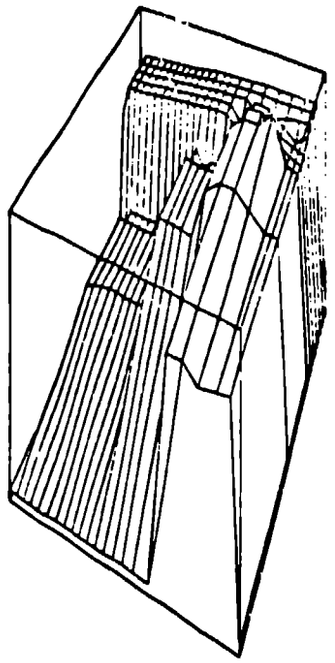

t = 1.1 s
(Min = 0.073, Max = 0.850)

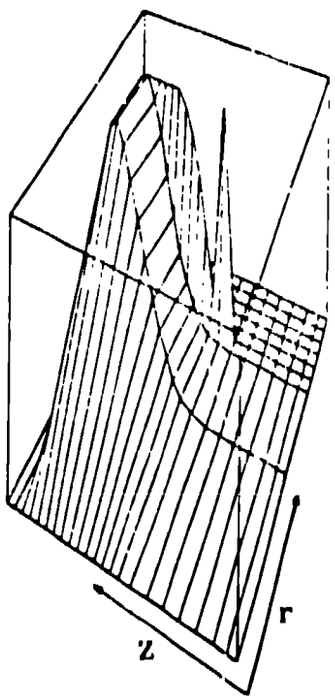

t = 0.1 s
(Min = 0., Max = 5768.)

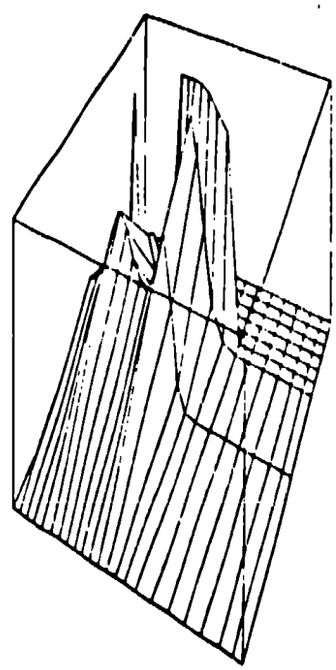

t = 1.1 s
(min = 0., Max = 5033.)

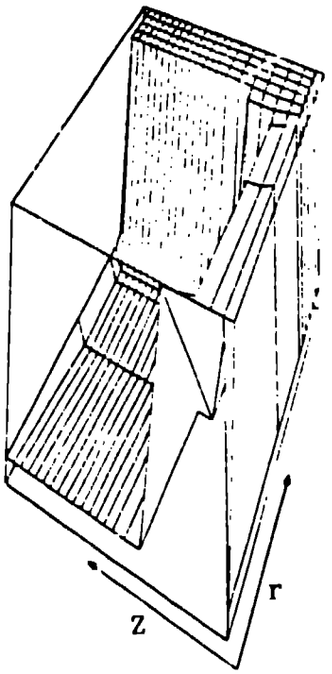

t = 0.1 s
(Min = 0., Max = 70.3)

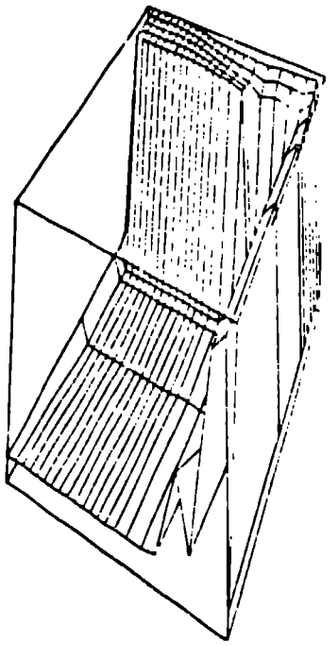

t = 1.1 s
(Min = 0., Max = 70.4)

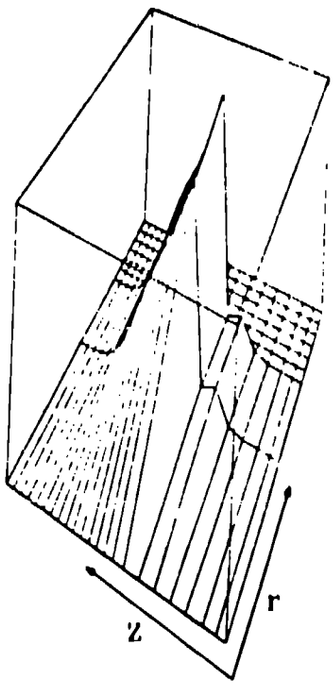

t = 0.1 s
(Min = 0., Max = 0.278)

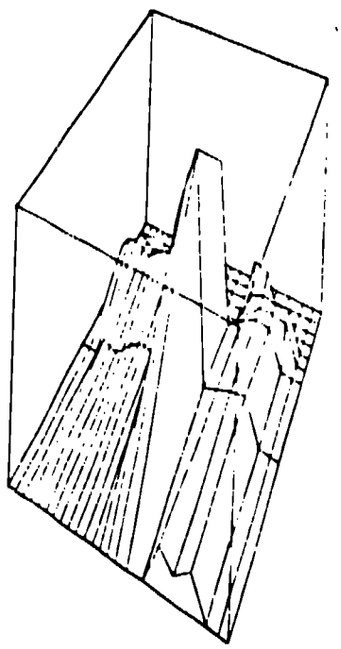

t = 1.1 s
(Min = 0., Max = 0.719)

Fig. 8.

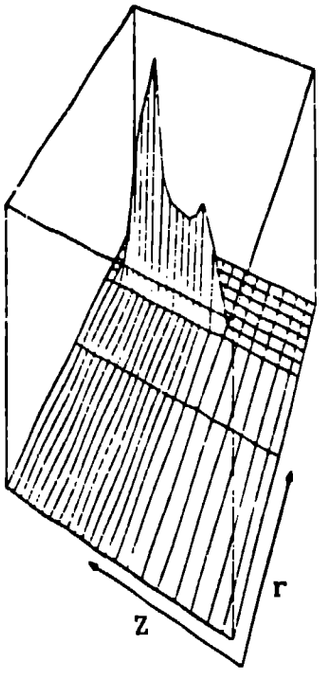

t = 0.1 s
(Min = 0., Max = 44.5)

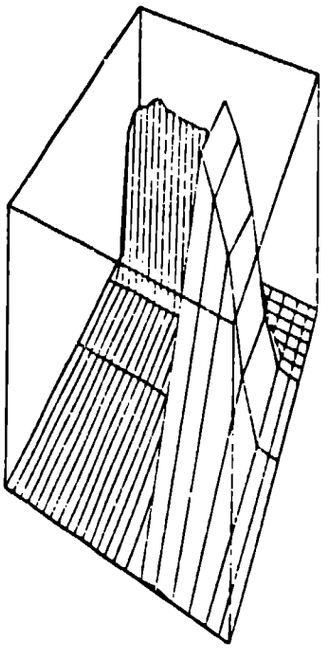

t = 1.1 s
(Min = 0., Max = 240.)

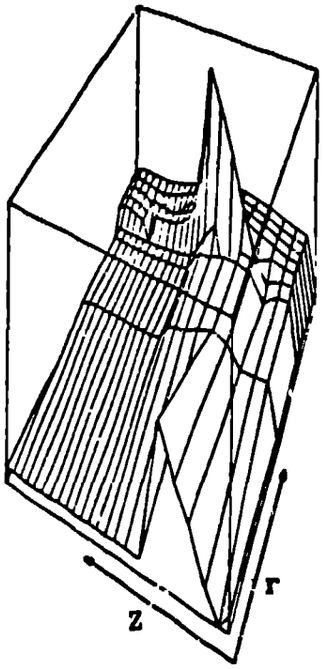

(a) Pressure (MPa)
(Min = 0.03, Max = 1.40)

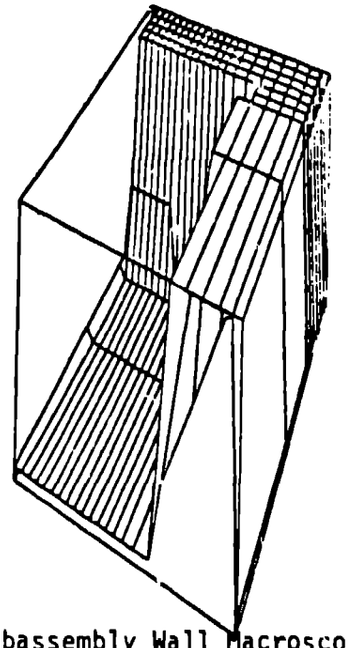

(b) Subassembly Wall Macroscopic Density (kg/m^3)
(Min = 0., Max = 2194.)

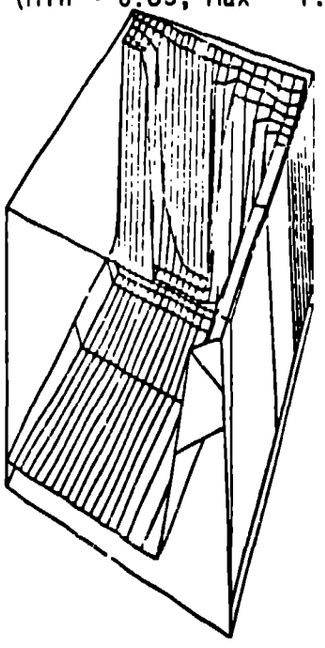

(c) Liquid Sodium Macroscopic Density (kg/m^3)
(Min = 0., Max = 70.2)

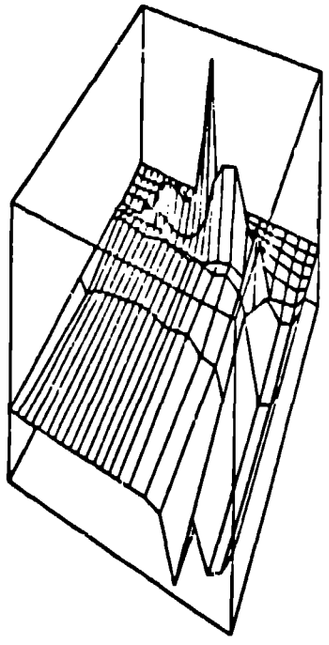

(d) Liquid Field Radial Velocity (m/s)
(Min = -10.8, Max = 31.6)

Fig.10.

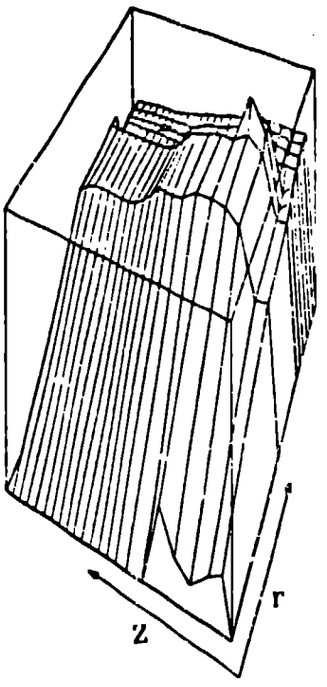

t = 1.5 s
(Min = 0.10, Max = 0.36)

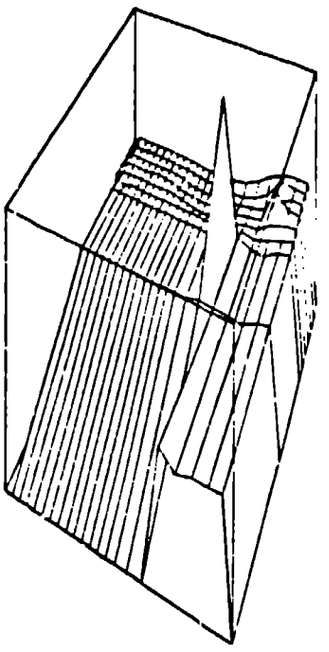

t = 1.9 s
(Min = 0.10, Max = 2.55)

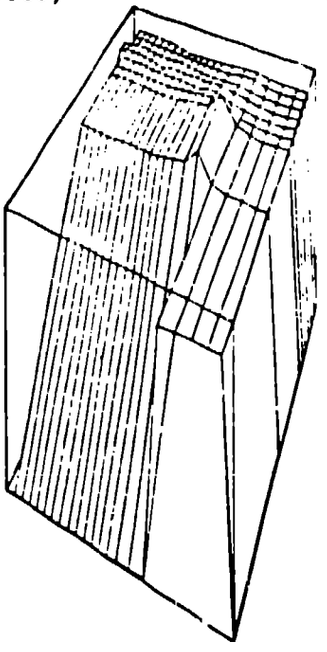

t = 4.1 s
(Min = 0.10, Max = 1.53)

Fig. 11.

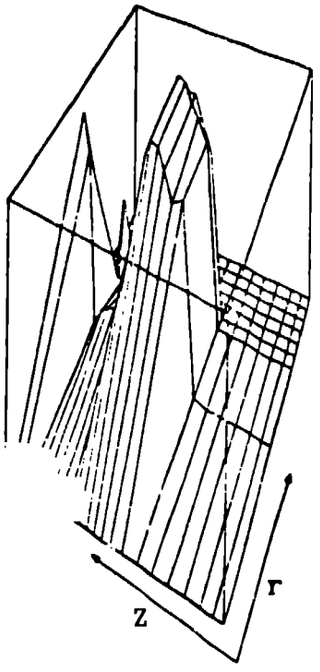

t = 1.5 s
(Min = 0., Max = 3045.)

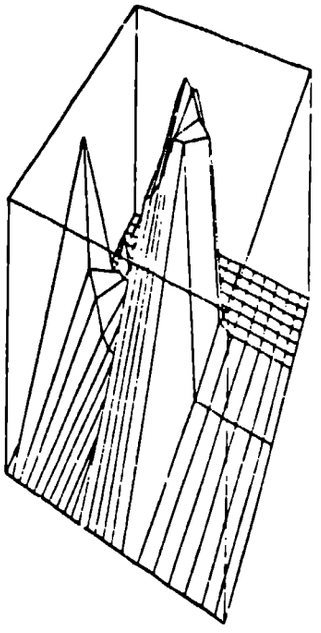

t = 1.9 s
(Min = 0., Max = 2952.)

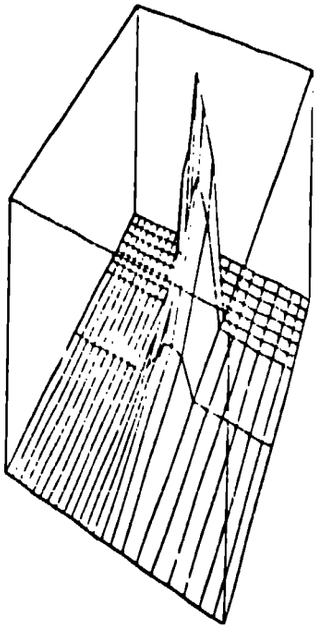

t = 4.1 s
(Min = 0., Max = 1471.)

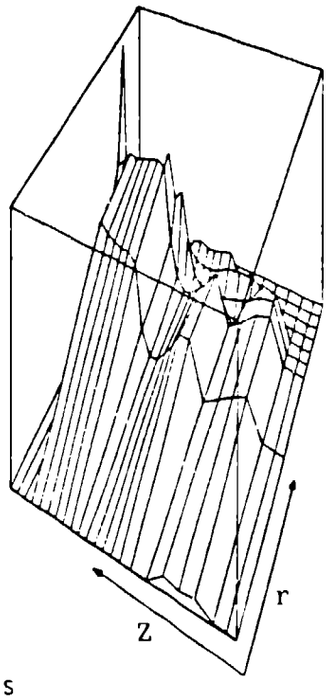

t = 1.5 s
(Min = 0., Max = 0.29)

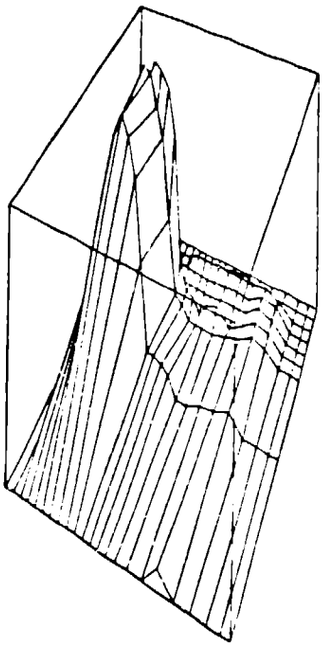

t = 1.9 s
(Min = 0., Max = 1.92)

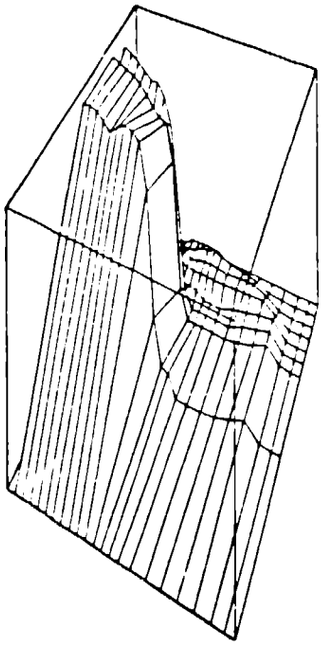

t = 4.1 s
(Min = 0., Max = 2.74)

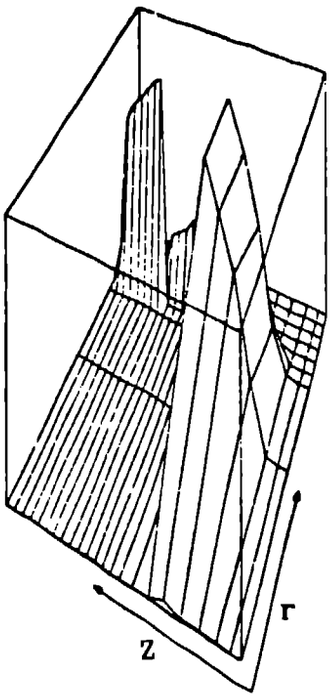

t = 1.5 s
(Min = 0., Max = 282.)

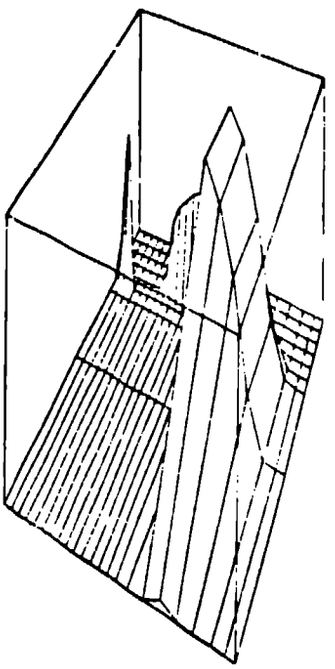

t = 1.9 s
(Min = 0., Max = 346.)

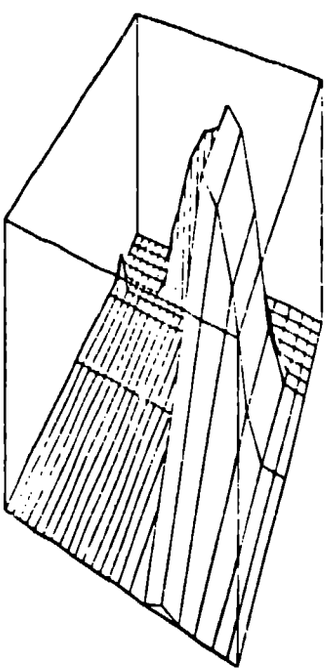

t = 4.1 s
(Min = 0., Max = 511.)

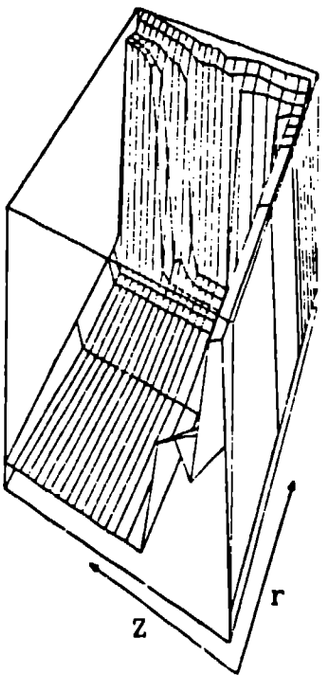

t = 1.5 s
(Min = 0., Max = 69.7)

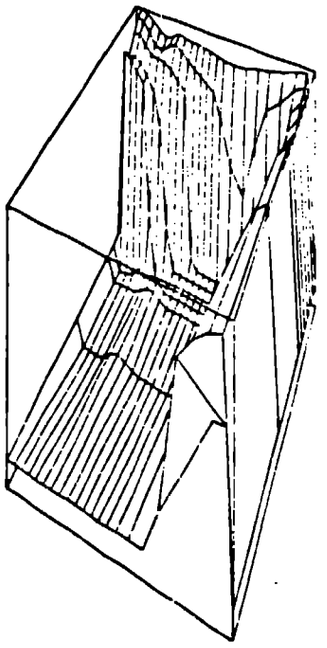

t = 1.9 s
(Min = 0., Max = 67.5)

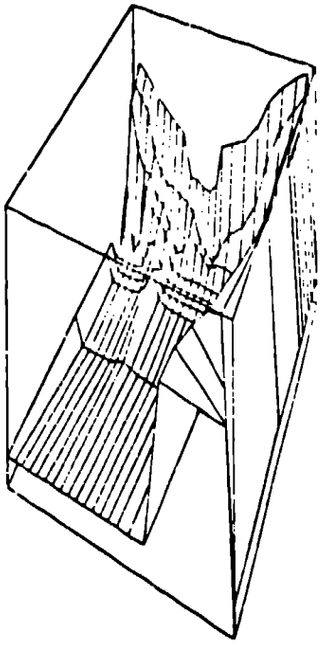

t = 4.1 s
(Min = 0., Max = 60.3)

Fig. 15.

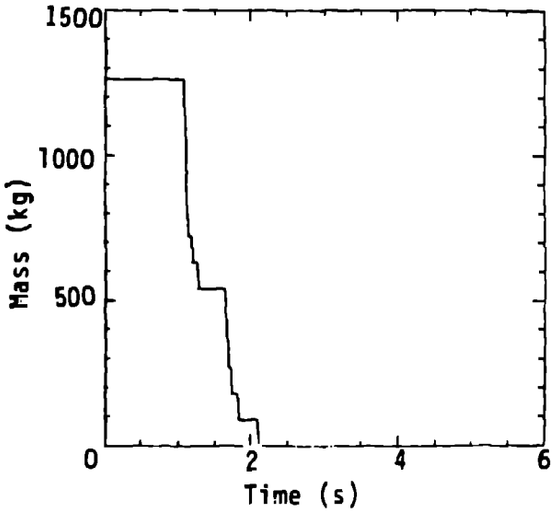

(a) Subassembly Wall
(Outer Core)

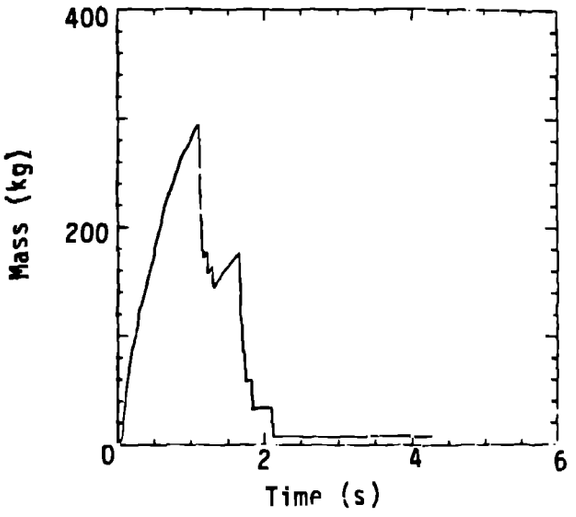

(b) Fuel Crust
(Core and Condenser Walls)

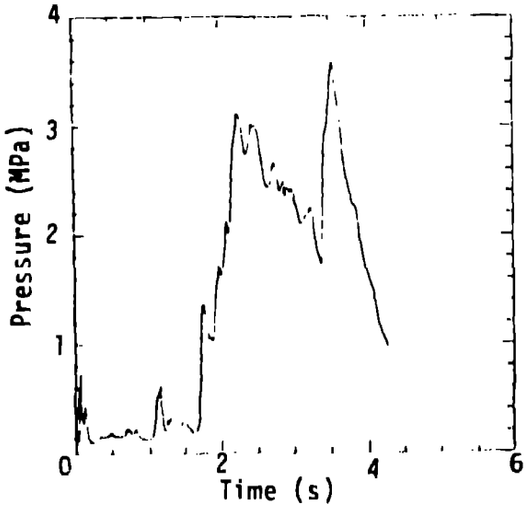

(c) Average Pressure
(Outer Core)

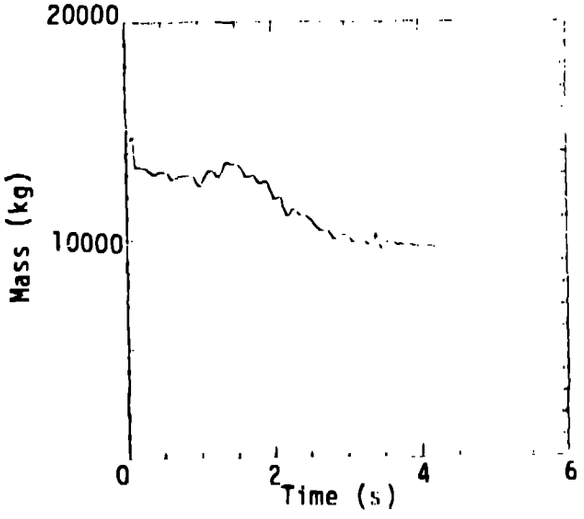

(d) Total Fuel
(Core)

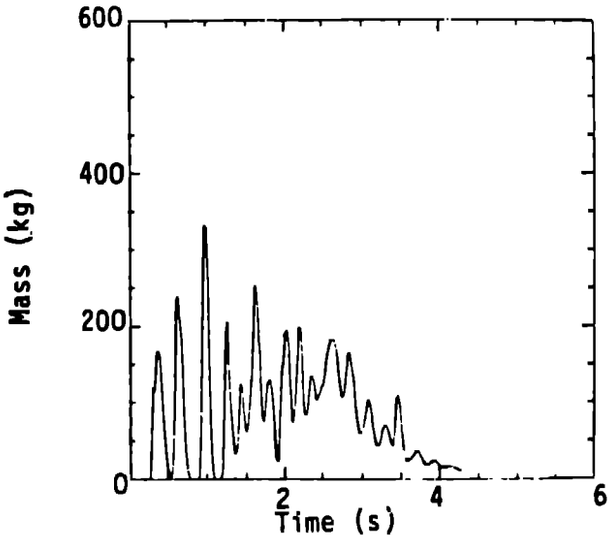

(a) Liquid Fuel
(Total Porous Region)

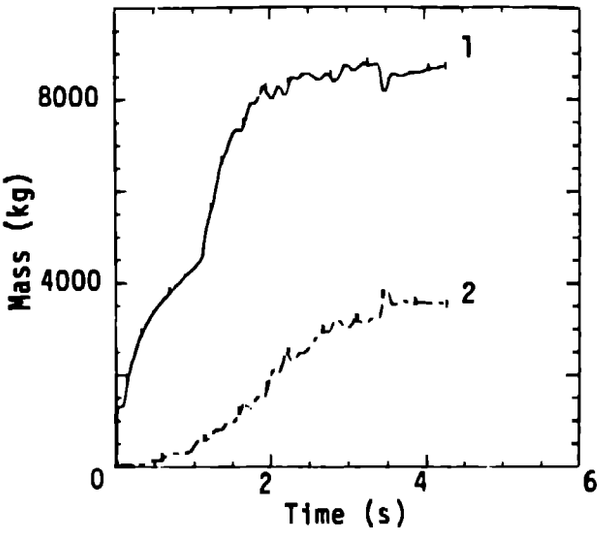

(b) Fuel Particles
(1 = Core and Condenser)
(2 = Total Porous Region)

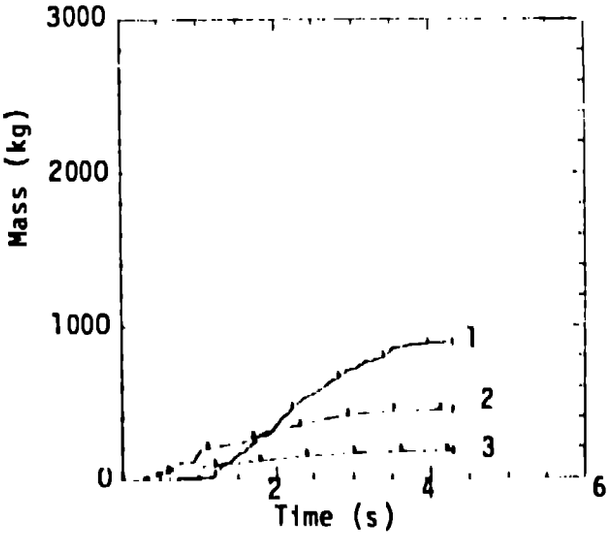

(c) Fuel Crusts
(1 = Porous Radial Blanket)
(2 = Porous Lower Assemblies)
(3 = Porous Below Core)

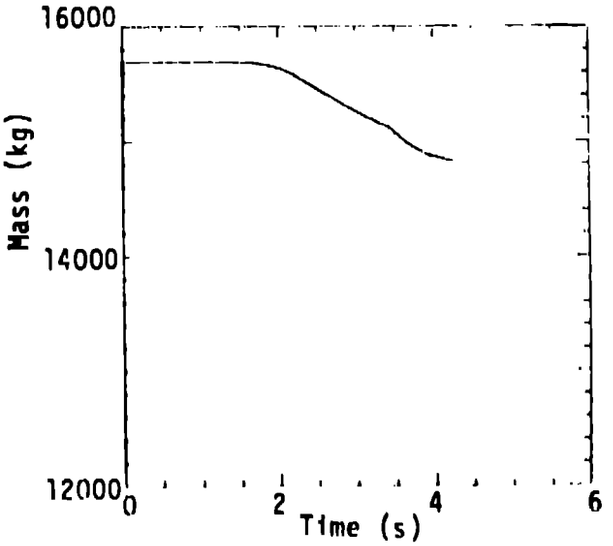

(d) Total Fuel Mass
(Total System)

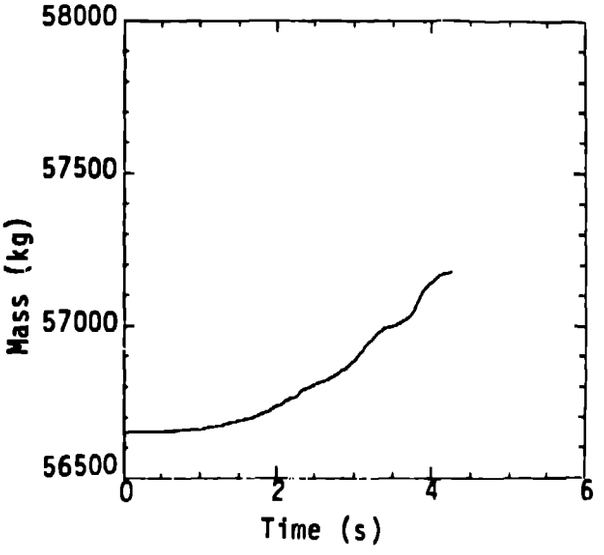

(a) Subassembly Wall
(Total Porous Region)

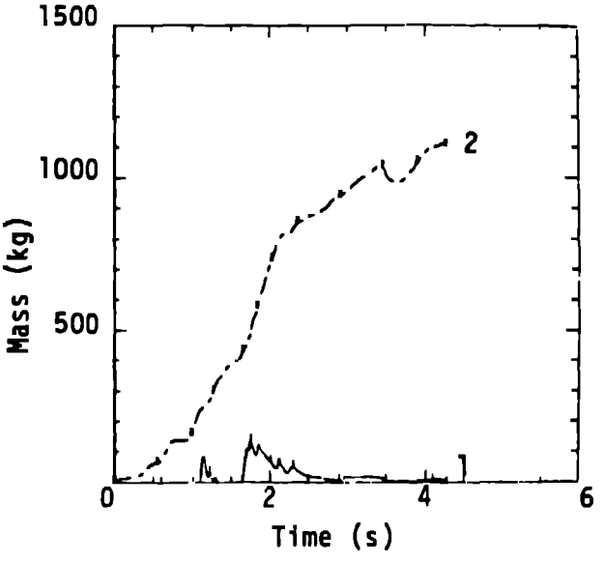

(b) Steel Particles
(1 = Core and Condenser)
(2 = Total Porous Region)

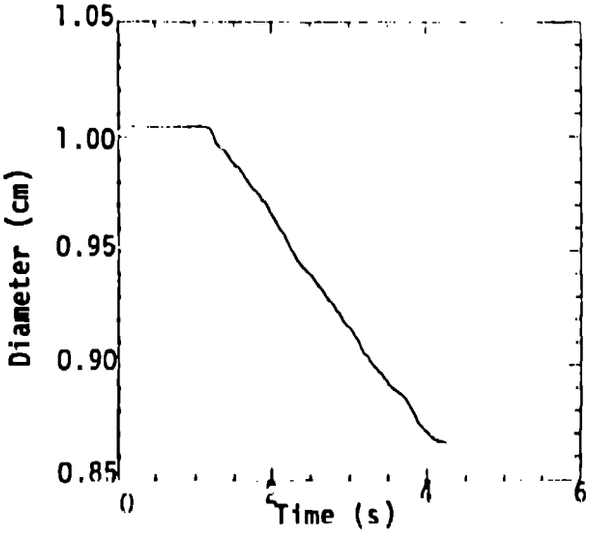

(c) Average Hydraulic Diameter
(Porous Radial Blanket)

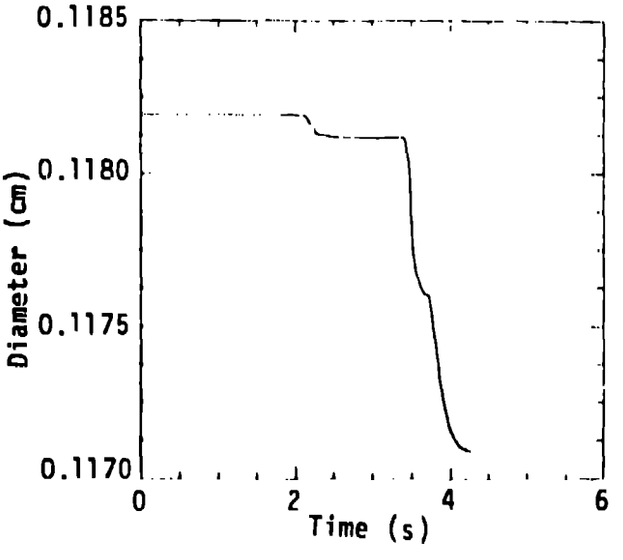

(d) Average Hydraulic Diameter
(Upper Leak Path)